

TRIM PERFORMANCE EXPLORATION FOR AN AIRCRAFT WITH DISTRIBUTED ELECTRIC PROPULSION AND A TAIL THRUST UNIT

Guilherme Fernandes Lourenço & Carmine Varriale

Delft University of Technology, Faculty of Aerospace Engineering, Delft, The Netherlands

Abstract

Trim performance for a commuter aircraft with wing-mounted Distributed Electric Propulsion (DEP) and a Horizontal Tail Thrust Unit (HTU) is investigated for steady level flight over the airspeed envelope. Attention is placed on how the redundancy in control effectors can be exploited to optimize different performance metrics. Three powertrain configurations are considered, in particular: HTU only, DEP only, and DEP+HTU. The effects of propulsion architecture on minimum trim speed, aerodynamic and electric power requirements, and key performance metrics are assessed. Results show that most of the reduction in minimum trim airspeed is obtained when DEP is activated, whereas only a marginal additional reduction is obtained when HTU is coupled with DEP. Minimum electric power is obtained with low angles of attack and small control surface deflections, with HTU acting as the main thrust source when available. Best range performance is obtained with similar trim attitudes, but flap settings are strongly affected by powertrain architecture. The DEP+HTU coupling results in the strongest increase of trimmed lift-to-drag ratio, though with the HTU acting as an air break. Reduced analytical relations based on linear lift-curve and parabolic drag-polar assumptions are fitted to the trim results to discuss high-level effects of the trim controls on the aerodynamic performance of the aircraft.

Keywords: Distributed Electric Propulsion, Trim Optimization, Aircraft Performance, Flight Mechanics

List of Symbols

D	Drag (N)
$\overline{E}$	Specific endurance $(1/\mathrm{W})$
K	Induced drag factor
L	Lift (N)
P	Power (W)
$\overline{R}$	Specific range $(1/\mathrm{N})$
S	Wing area (m^2)
T	Thrust (N)
V	Airspeed $(\mathrm{m/s})$
W	Weight (N)
p, q, r	Angular rate comp. $(\mathrm{rad/s})$
u, v, w	Velocity components $(\mathrm{m/s})$
α	Angle of attack (rad)
γ	Flight path angle (rad)
δ	Control input
η	Efficiency
θ	Pitch angle (rad)
ρ	Air density $(\mathrm{kg/m}^3)$
τ	Flap effectiveness

Subscripts

$\mathrm{a, e, s}$	Aerodynamic, electric, shaft
$\mathrm{f, r}$	Flap, ruddervator
$\mathrm{lb, ub}$	Lower and upper bounds
tr	Trim

1. Introduction

Emerging aircraft configurations featuring wing-mounted Distributed Electric Propulsion (DEP) are characterized by strongly coupled aero-propulsive phenomena [1–3]. This interaction entirely characterizes the flight performance of these aircraft, making the analysis and optimization of different

https://doi.org/10.71945/icas2026_0377

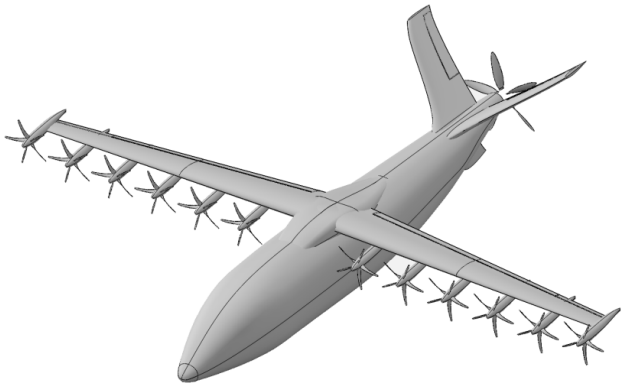


Figure 1 – Geometry of the UC7A in OpenVSP [12].

Table 1 – Configuration parameters of the UC7A [15].

Parameter	Value
Mass	7438 kg
CG longitudinal position	8.32 m
CG vertical position	0.20 m
Wing area	30 m^2
Wing span	20.11 m
Wing chord	1.43 m

performance metrics significantly more challenging [4]. In a blown-lift DEP configuration, for example, the propulsion system is distributed along the leading edge of the wing in order to take advantage of the accelerated flow over the wing sections behind the engines. This arrangement increases the lift capability of the wing, and energizes the boundary layer, allowing for the reduction of the overall wing size without causing earlier stall onset [5, 6].
Identifying the trim states and controls for such a complex system in various flight conditions is not a trivial problem, as the available degrees of freedom are redundant and also coupled. The possibility to use different thrust settings on each propeller increases the number of trim controls, making the trim problem under-determined [7, 8]. This creates the conditions for multiple trim solutions to exist for the same flight condition, which can be exploited to optimize the aircraft performance [9–11]. Typical limiting factors for trimming a tube-and-wing aircraft configuration at the boundaries of the flight envelope are the available power, the maximum lift coefficient, and the maximum elevator deflection. It is then interesting to explore the possibility to improve trimmed aircraft performance by exploiting the redundancy of different propulsive units, in combination with other aerodynamic effectors.
This paper presents a methodology to explore trim solutions for an aircraft with a blown-lift DEP system and additional Horizontal Thrust Unit (HTU). It also provides simplified relations between the required aerodynamic power and various trim variables, which could be used as a surrogate model for rapid performance assessment.

2. Reference aircraft

The proposed methodology is applied to the Unifier C7A-HARW (UC7A), shown in Figure 1. This is a 19-passenger hybrid-electric commuter aircraft featuring a DEP system on the main wing and a HTU behind the tail [12–14]. It features a tapered, slender wing, with a straight leading edge and a slight anhedral angle, attached to the upper part of the fuselage and equipped with a flap, an aileron, and 6 fixed-pitch foldable high-lift propellers on each side. Aft of the main wing, a V-tail is equipped with two ruddervators, and the variable-pitch propeller HTU is mounted on the rear of the fuselage.
The flight mechanics model of the UC7A that is used for the current work is retrieved from [15, 16]. It is a six-degrees-of-freedom rigid body model implemented in MATLAB Simulink. The aero-propulsive forces are calculated by interpolating precomputed databases, obtained with multi-fidelity CFD simulations, comprising panel methods and Reynolds-averaged Navier-Stokes (RANS) simulations. The wings and tail surfaces are split into sections, for which the aerodynamic coefficients and downwash effects are tabulated as a function of the local flight parameters. The blown-lift effect of the DEP system is included in the aerodynamic coefficients of the wing sections, while the HTU has no effect on the airframe aerodynamics.
As inputs, the DEP and HTU models receive thrust "activity factors" δ_{T_i}. Each DEP propeller can generate a maximum thrust of $800\,\mathrm{N}$, and any thrust lower than $0.8\,\mathrm{N}$ is overridden to zero. The HTU can generate both positive (forward) and negative (reverse) thrust, from $-5000\,\mathrm{N}$ to $15\,000\,\mathrm{N}$, depending on the airspeed and according to the motor's operating limits.

3. Methodology

Two main trimming problem formulations are explored. In both formulations, $\dot{x}_\mathrm{k}$ represents the array of body-axis translational and rotational accelerations (Equation 1), and $\boldsymbol{\lambda}$ is the array of decision variables that the trim optimizer varies to search for trim conditions. These "trim controls" are constituted, in this study, by airspeed, angle of attack, flap and ruddervator deflections, and thrust activity factors (Equation 2). Only symmetric deflections and thrust settings are considered for the DEP propellers and control surfaces, while ailerons are always set to zero.

$$\dot{x}_\mathrm{k} = [\dot{u}, \dot{v}, \dot{w}, \dot{p}, \dot{q}, \dot{r}]^T \tag{1}$$

$$\boldsymbol{\lambda} = [V, \alpha, \delta_\mathrm{f}, \delta_r, \delta_{T_i}, \delta_{T_\mathrm{HTU}}]^T \quad \text{with } i = 1, ..., 6 \tag{2}$$

A generic trim problem is cast as the minimization of translational and rotational accelerations (Equation 3).

$$\begin{aligned} \min_{\boldsymbol{\lambda}} \quad & \mathcal{J} = \dot{x}_\mathrm{k}^T \dot{x}_\mathrm{k} \\ \text{subject to} \quad & \boldsymbol{\lambda}_\mathrm{lb} \leq \boldsymbol{\lambda} \leq \boldsymbol{\lambda}_\mathrm{ub} \end{aligned} \tag{3}$$

An additional trim problem is formulated to find the minimum airspeed while subject to steady level flight constraints (Equation 4), given the available control surfaces and thrust settings.

$$\begin{aligned} \min_{\boldsymbol{\lambda}} \quad & \mathcal{J} = V \\ \text{subject to} \quad & \dot{x}_\mathrm{k} = 0 \\ & \boldsymbol{\lambda}_\mathrm{lb} \leq \boldsymbol{\lambda} \leq \boldsymbol{\lambda}_\mathrm{ub} \end{aligned} \tag{4}$$

The trim controls are bounded by the values reported in Table 2, and are normalized as in Equation 5.

$$\hat{\lambda}_i = \frac{\lambda_i - \lambda_{\mathrm{lb},i}}{\lambda_{\mathrm{ub},i} - \lambda_{\mathrm{lb},i}} \tag{5}$$

In all cases, the accelerations resulting from the combination of trim controls are calculated, at every optimizer iteration, via simulation of the flight mechanics model in Simulink. The optimization problem is solved with MATLAB `fmincon` function, with the settings reported in Table 3. Every trim problem simulation is repeated 500 times, with randomized initial conditions, to explore the entire solution space and identify multiple trim solutions when they exist.

Table 2 – Trim control bounds.

Parameter	V (m/s)	α (deg)	δ_f (deg)	δ_r (deg)	δ_{T_i}	δ_{T_HTU}
Bounds	$[0, 89]$	$[-15, 20]$	$[0, 25]$	$[-30, 15]$	$[0, 1]$	$[-0.5, 1.5]$

Table 3 – Solver settings for the `fmincon` function.

Algorithm	**TolFun**	**TolX**	**FinDiffType**	**DiffMinChange**	**DiffMaxChange**
sqp	1×10^{-10}	1×10^{-10}	central	1×10^{-10}	0.5

Three combinations of usage of the DEP and HTU systems are examined to assess the variation in trim controls and trimmed flight performance under different propulsive constraints. The corresponding test cases are listed in Table 4. In case 1 (OHTU), only the HTU is active: this is the most conventional case, as there is no redundancy in the trim controls and also no aero-propulsive interaction with the airframe. Case 2 (ODEP) features only DEP being active, introducing redundant controls and aero-propulsive coupling. Case 3 (DEP+HTU) is the most general one, as is defined by active HTU and DEP operation without additional constraints beyond their respective operating limits. In all cases, trim is conducted for symmetric horizontal flight at sea-level altitude, with aircraft parameters as indicated in Table 1.

Table 4 – Fixed and free trim controls for every test case.

Case	Active propulsion	Trim objective	Trim controls	Assigned variables
1	HTU	Minimum V Trim at assigned speed	$V,\ \alpha,\ \delta_\mathrm{f},\ \delta_\mathrm{r},\ \delta_{T_\mathrm{HTU}}$ $\alpha,\ \delta_\mathrm{f},\ \delta_\mathrm{r},\ \delta_{T_\mathrm{HTU}}$	$\delta_{T_i} = 0\ \forall i$ $V = 0,\ \delta_{T_i} = 0\ \forall i$
2	DEP	Minimum V Trim at assigned speed	$V,\ \alpha,\ \delta_\mathrm{f},\ \delta_\mathrm{r},\ \delta_{T_i}$ $\alpha,\ \delta_\mathrm{f},\ \delta_\mathrm{r},\ \delta_{T_i}$	$\delta_{T_\mathrm{HTU}} = 0$ $V = 0,\ \delta_{T_\mathrm{HTU}} = 0$
3	DEP + HTU	Minimum V Trim at assigned speed	$V,\ \alpha,\ \delta_\mathrm{f},\ \delta_\mathrm{r},\ \delta_{T_i},\ \delta_{T_\mathrm{HTU}}$ $\alpha,\ \delta_\mathrm{f},\ \delta_\mathrm{r},\ \delta_{T_i},\ \delta_{T_\mathrm{HTU}}$	— V

Relevant aircraft performance indicators, such as specific range, specific endurance and lift-to-drag ratio are obtained from numerical simulations, using Equations 6. The efficiencies of the electric motors η_motor and power-controller $\eta_\mathrm{controller}$ are 0.95 and 0.97, respectively [13].

$$P_\mathrm{e} = P_{\mathrm{HTU_e}} + P_{\mathrm{DEP_e}} = \eta_\mathrm{motor}\eta_\mathrm{controller}(P_{\mathrm{HTU_{shaft}}} + P_{\mathrm{DEP_{shaft}}}) \tag{6a}$$

$$P_\mathrm{a} = VD \tag{6b}$$

$$\overline{E} = 1/P_\mathrm{e} \tag{6c}$$

$$\overline{R} = V/P_\mathrm{e} \tag{6d}$$

4. Results

For the aircraft to be trimmed, the lift force must be equal in magnitude to the weight and, therefore, constant. The total aircraft lift is generated by the airframe and the propulsion system in different proportions and with very different possible combinations of control inputs. Moreover, thrust generated by the DEP system contributes significantly to both horizontal and vertical equilibrium in light of its strong blown-lift capabilities, which are also dependent on the angle of attack and flap deflection.
The following subsections explore the trim solution space for the different powertrain configurations, and the resulting performance in terms of minimum trim speed, aerodynamic power required, and key performance metrics.

4.1 Minimum Airspeed

The minimum trimmed airspeeds and corresponding airframe trim control values for each of the propulsion configurations are shown in Table 5 for the different test cases. The ODEP minimum trim airspeed V_min is 11.5% lower than the OHTU one, and it is further reduced by just 0.6% in the DEP+HTU case. This suggests that using DEP is essential to reducing V_min, but coupling DEP and HTU has little effect. The flap is always deflected at its maximum $25\,\mathrm{deg}$, and the angle of attack is always around $12\,\mathrm{deg}$, which are the wing trim controls for maximum lift coefficient. In no case the ruddervator deflection δ_r is being limited by its bounds, suggesting that this aircraft configuration always has enough pitch moment control authority at minimum speed.
Figure 2 shows the range of values for the DEP and HTU activity factors at minimum trim speed for each test case. The OHTU solution is uniquely determined by the highest lift coefficient of the wing, with the HTU mainly counteracting the resultant drag force and the ruddervator adjusting for pitch moment. For the ODEP case, the three most inboard propellers operate at the maximum activity factor of 1, while the other ones operate in a lower range of activity factors, which get closer to 0 approaching the wing tip. For the DEP+HTU case, all propellers operate at $\delta_T = 1$, apart from the wing-tip one which operates at activity factors from almost 0 all the way to 1. This is regulated by some variability in the angle of attack and ruddervator deflection. The HTU is always operating in the negative thrust regime, acting therefore as a drag generator, but is never limited by its bounds.
This behaviour is explained by the fact that the wing-tip propeller contributes to thrust just as all the others, but has less impact on lift since the portion of the wing it blows onto is smaller. In this way, when paired to an HTU that can act as an air brake, the wing-tip propeller gets used to partially decouple the horizontal and vertical equilibrium constraints: it allows the inboard propellers to operate at maximum activity factor for maximum lift generation, and balances the horizontal forces together with the HTU, while the ruddervator takes care of trimming the pitch moment.

Table 5 – Minimum trimmed airspeed and corresponding range of values of airframe trim controls, for different test cases.

Powertrain	$V_{\min}$ (m/s)	α (deg)	δ_{f} (deg)	δ_{r} (deg)
OHTU	38.3	12	25	-10.1
ODEP	33.9	12	25	[-16.6, -15.7]
DEP+HTU	33.7	[11.8, 12]	25	[-17.8, -16]

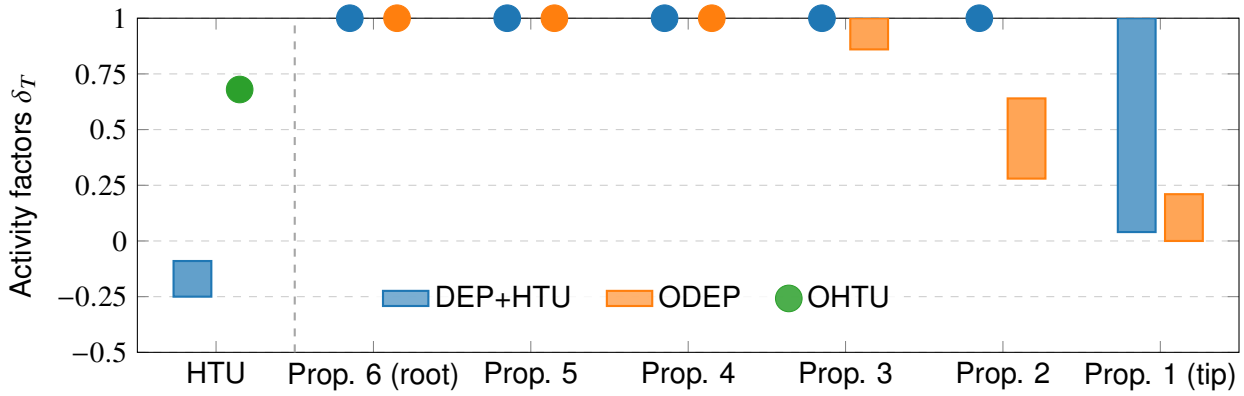


Figure 2 – DEP and HTU activity factors at minimum trimmed airspeed. Floating bars span the range of feasible trim solutions; markers indicate a unique trim value.

4.2 Performance Diagrams

Figure 3 shows the aerodynamic power required by the OHTU configuration to trim at different airspeeds, with the angle of attack and flap deflection as color bars. The ruddervator deflection reflects the trend of the angle of attack (with appropriate sign and scaling), and is not reported for brevity. Despite this being the most conventional propulsion configuration, different combinations of angle of attack, flap deflection, and ruddervator deflection allow for a wide range of trim solutions at most given airspeeds.

The trim optimizer correctly captures the expected trend of decreasing angle of attack and flap deflection with increasing airspeed, for minimum aerodynamic power. At high speeds, the two trim controls can be somewhat traded off against each other: at a given speed, multiple solutions exist with small or negative angles of attack, and corresponding null or positive flap deflection. Low airspeeds are instead characterized by the angle of attack being positive, with the flap being the primary control to enable their decrease.

At low and high airspeeds, this redundancy in trim controls results in a wide spread of values of the required aerodynamic power. The maximum and minimum angles of attack achievable in trim are indeed limited not only by the bounds on flap deflection, but also on the power made available by the HTU. In the regime around the airspeed for maximum lift-to-drag ratio V_{LDmax}, required aerodynamic power is more narrowly defined, despite the still significant excursion in angle of attack and flap deflection.

Similar considerations can be made for the ODEP powertrain, shown in Figure 4. It may be interesting to note that maximum angle of attack achievable in this case is of $16\,\mathrm{deg}$, as compared to the one of $18\,\mathrm{deg}$ achieveable in the OHTU case. This is a consequence of the lower installed available power at low speeds, and possibly also of the fact that the DEP propellers are installed with a negative incidence angle of $-5\,\mathrm{deg}$ with respect to the wing chord.

For the DEP+HTU case, shown in Figure 5, trim solutions are never restricted by the available power, but only by the trim controls bounds. Trimming the aircraft for minimum aerodynamic power requires negative angles of attack at high airspeeds, which may indicate that lifting surfaces are slightly oversized for flight in these conditions.

Once again, the aerodynamic power required to fly at airspeeds around the one for maximum lift-to-drag ratio is confined in a very narrow range. In this speed regime, trim is possible for both the

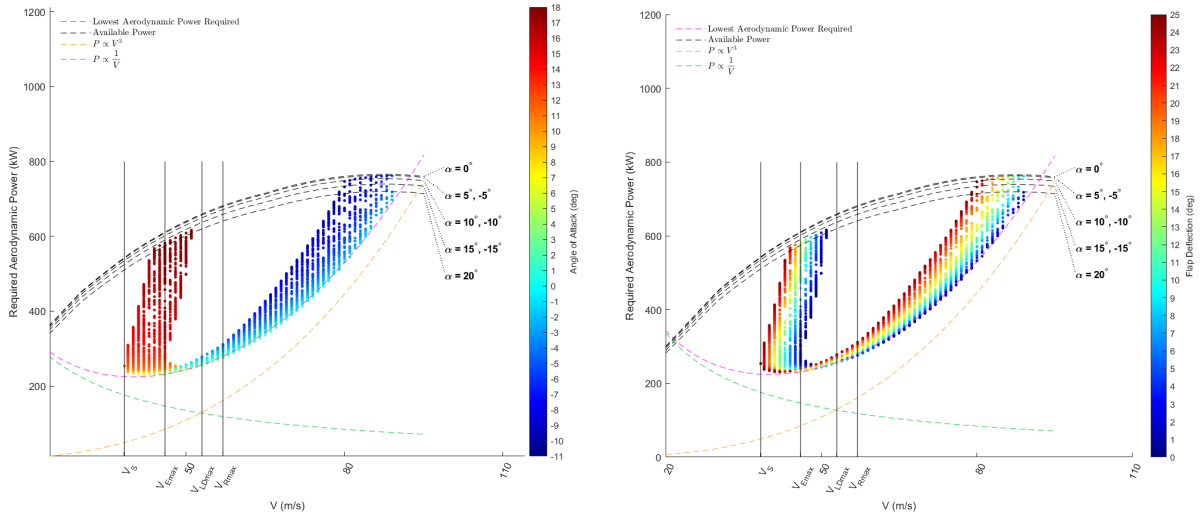


Figure 3 – Required aerodynamic power in trim as a function of airspeed, using OHTU. Colour bars indicate the angle of attack (*left*) and flap deflection (*right*).

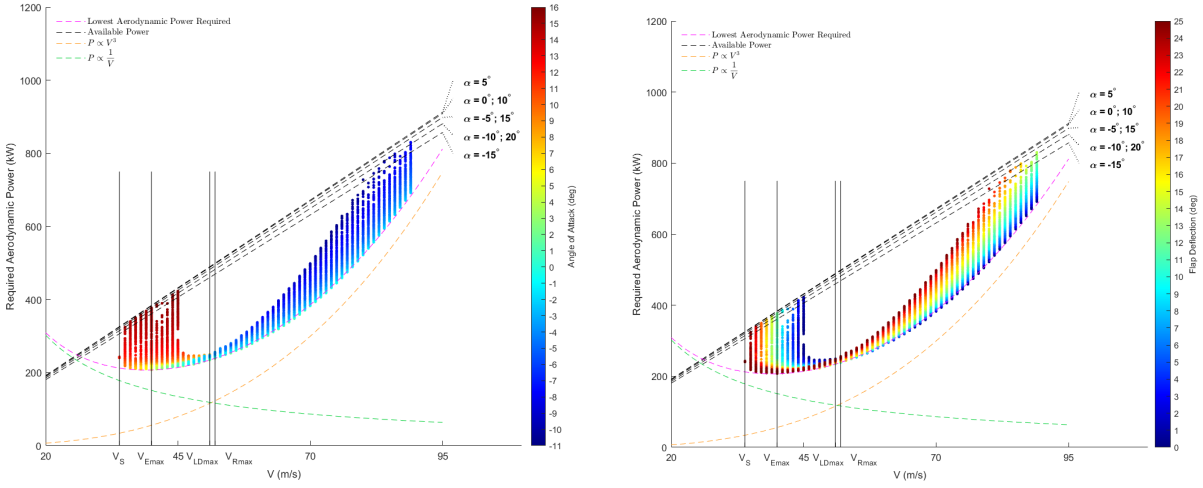


Figure 4 – Required aerodynamic power in trim as a function of airspeed, using ODEP. Colour bars indicate the angle of attack (*left*) and flap deflection (*right*).

maximum and minimum flap deflections with roughly the same P_a. The trim point with the maximum δ_f has a negative α and the DEP system is producing more thrust force than the HTU, while the trim point with the minimum δ_f has a positive α and the HTU is producing more thrust than the DEP.
As shown in the bottom-right panel of Figure 5, the electrical power used P_e increases with the required aerodynamic power P_a, in general. However, the minimum P_a at some airspeed does not coincide with the minimum P_e. This happens when the DEP system is used to improve the aerodynamic performance of the aircraft, and/or when the HTU generating negative/reverse thrust, at the expense of a higher electric power consumption. For example, at the overall minimum aerodynamic power required, while inboard DEP propellers contribute to the thrust and lift budget for horizontal and vertical equilibrium, the wing-tip propeller operates (together with the HTU) primarily as a thrust source rather than a lift augmentation device. In this regime, its slipstream attenuates the wing-tip vortex, thereby reducing induced drag and P_a, but consuming more P_e.

4.3 Performance Metrics (PMs)

The best trimmed PMs across the three powertrains are compared in Table 6, and the corresponding trim controls are given in Table 7. In every case, the three best trim solutions for each configuration

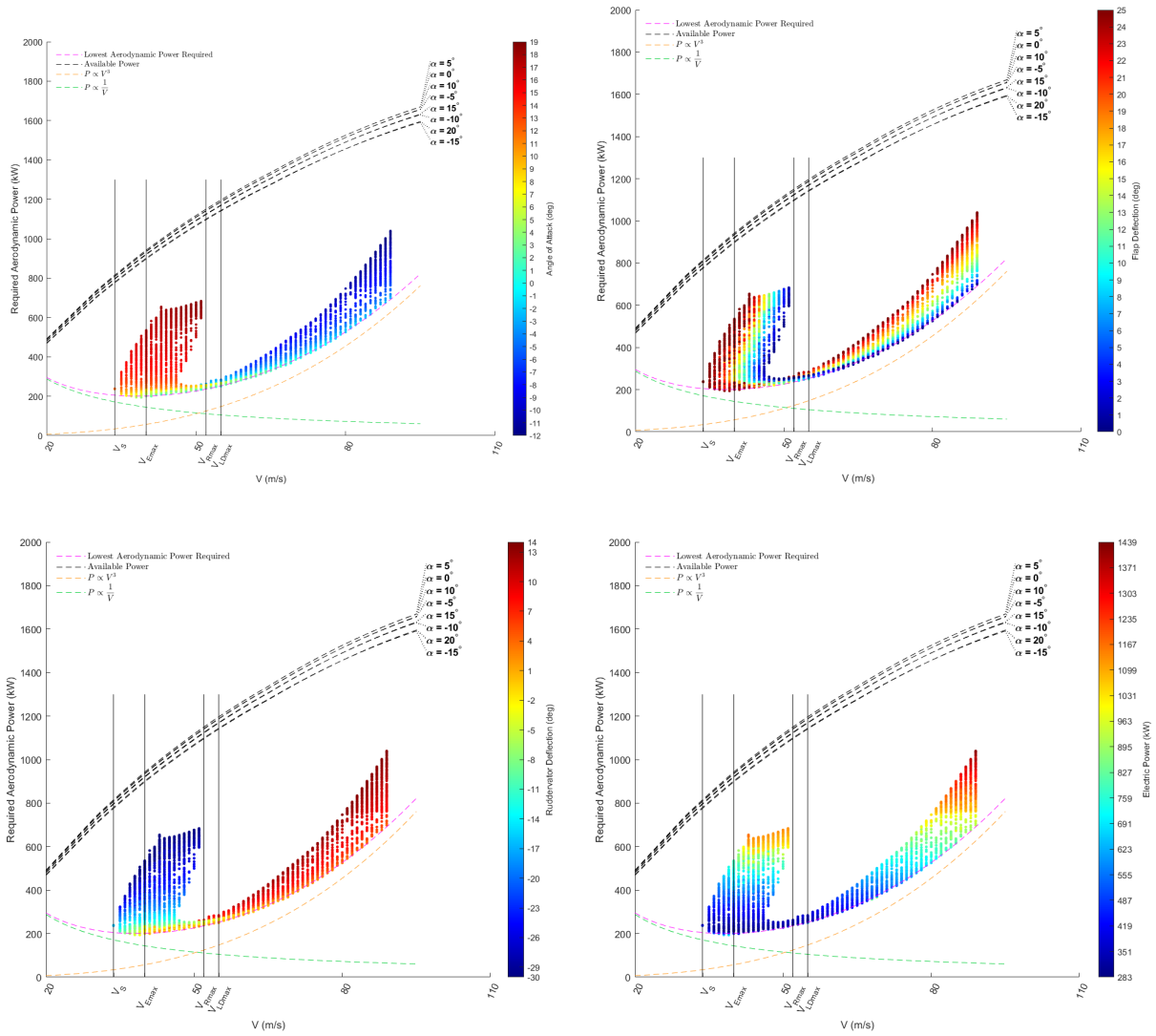


Figure 5 – Required aerodynamic power in trim as a function of airspeed, using DEP+HTU. Colour bars indicate angle of attack (*top left*), flap deflection (*top right*), ruddervator deflection (*bottom left*), and electric power consumed (*bottom right*).

Table 6 – Best trimmed PMs by test case; changes are relative to OHTU.

Powertrain	Max $\overline{R}$ $(1/\mathrm{kN})$	Max L/D	Max $\overline{E}$ $(1/\mathrm{kW})$	Min P_e (kW)
OHTU	0.162	15.1	3.17×10^{-3}	315
ODEP	0.168 (+4%)	16.0 (+6%)	3.61×10^{-3}	277 (−12%)
DEP+HTU	0.165 (+2%)	20.6 (+36%)	3.53×10^{-3}	283 (−10%)

and objective are nearly identical, so a single representative set of values is reported.

From Table 6, using DEP alone can improve all three indicators over OHTU. ODEP can achieve the best specific range (+4%) and the lowest P_e (-12%), while DEP+HTU can reach a substantially higher maximum L/D of 20.6. This is thanks to the excess power available and the redundancy in the controls, but comes at the cost of a slightly inefficient use of electric power installed.

For maximum specific range, all three configurations favour low positive angles of attack and low-to-intermediate flap deflections with near-zero ruddervator input. For maximum L/D, an angle of attack near $1\,\mathrm{deg} - 3\,\mathrm{deg}$ and an intermediate flap deflection near $10\,\mathrm{deg}$ are found to be ubiquitously desirable; in the DEP+HTU case, very high DEP thrust settings are coupled with a negative HTU thrust setting. Maximum specific endurance is reached at higher angles of attack, near $4\,\mathrm{deg} - 6\,\mathrm{deg}$, with maximum or near-maximum flap deflection and small negative ruddervator deflection.

Table 7 – Trim airspeed and corresponding trim controls for the best trimmed PMs by test case. Trim controls for maximum specific endurance correspond to those with minimum electric power consumption.

Powertrain	Objective	V (m/s)	α (deg)	δ_f (deg)	δ_r (deg)	δ_T
OHTU	Max $\overline{R}$	57 m/s	3	5	+1	$\delta_{T_\mathrm{HTU}} = 0.48$
	Max L/D	53 m/s	3	10	+2	$\delta_{T_\mathrm{HTU}} = 0.48$
	Max $\overline{E}$	46 m/s	6	15	−1	$\delta_{T_\mathrm{HTU}} = 0.51$
ODEP	Max $\overline{R}$	52 m/s	2	10	≈ 0	No clear spanwise trend in δ_{T_i}
	Max L/D	51 m/s	2	11	≈ 0	No clear spanwise trend in δ_{T_i}
	Max $\overline{E}$	40 m/s	4	25	−2	No clear spanwise trend in δ_{T_i}
DEP+HTU	Max $\overline{R}$	52 m/s	3	9	≈ 0	$\delta_{T_i} = 0$ or at max $\eta \approx 0.83$, $\delta_{T_\mathrm{HTU}} > 0$
	Max L/D	55 m/s	1	10	+1	δ_{T_i} high, $\delta_{T_\mathrm{HTU}} < 0$
	Max $\overline{E}$	40 m/s	5	25	−2	Wide range of $\{\delta_{T_i}, \delta_{T_\mathrm{HTU}}\}$ combinations

The DEP+HTU exhibits the widest diversity of behaviors in all cases, as expected. In the maximum range case, the DEP propellers are either turned off or operating at maximum propulsive efficiency, corresponding to an advance ratio of approximately 1.75. For the maximum endurance case, trim conditions with minimum electric power span a wide range of DEP and HTU thrust combinations, since the HTU can dissipate the same absolute electric power at either low thrust (and low efficiency) or at high thrust (and high efficiency). No clear spanwise DEP-thrust distribution was identified for any performance objective; however, prioritizing higher angles of attack over larger flap deflections with similar thrust distributions was found to increase specific range.

4.4 Aerodynamic Angles

The trim angle of attack, flap deflection, and ruddervator deflection at minimum P_a are now discussed in more detail. They are shown as a function of airspeed in Figure 6 for all three powertrain configurations. In all cases, the ruddervator deflection follows an inverse trend to the angle of attack, consistent with the pitch moment balance requirement.

For the OHTU case (above left), δ_flap is maintained constant over different ranges of airspeeds, with such constant value and the angle of attack decreasing for increasing airspeed. Since the HTU does not interact aerodynamically with the airframe, the minimum P_e trim controls are nearly identical to those at minimum P_a, and the corresponding thrust required for trim follows a parabolic relationship with airspeed consistent with a conventional drag polar.

For ODEP (above right) and DEP+HTU (below), flap deflection is within its bounds over an intermediate airspeed range. In this regime, the angle of attack remains approximately constant with flap deflection decreasing linearly from its maximum of $25\,\mathrm{deg}$ to zero. The equilibrium angle of attack stabilises between $2\,\mathrm{deg}$ and $3\,\mathrm{deg}$ for ODEP, and between $0\,\mathrm{deg}$ and $2\,\mathrm{deg}$ for DEP+HTU. This difference is attributed to the availability of the HTU as an additional thrust source: in the ODEP configuration, the horizontal equilibrium constraint limits DEP thrust to levels below which the aero-propulsive lift boost is fully exploited, requiring a slightly higher angle of attack. When HTU is coupled with DEP, the excess thrust can be absorbed by the HTU, allowing the DEP to operate at higher settings and the angle of attack to approach zero.

At low airspeeds (below approximately $43\,\mathrm{m/s}$), maximum flap deflection is saturated and the angle of attack decreases rapidly with increasing airspeed across all configurations. A similar behaviour is observed at high airspeeds (above approximately $68\,\mathrm{m/s}$), where the minimum flap deflection is reached, though the decrease of angle of attack is more gradual.

4.5 Reduced Aerodynamic Models

It is now interesting, from a conceptual point of view, to simplify the complex and coupled aero-propulsive model of this aircraft using trim constraints and results. The proposed approach involves abstracting the aerodynamic contributions of the different components of the aircraft (movable surfaces, DEP and HTU throttles) into an integrated aerodynamic model, consisting of only the airframe

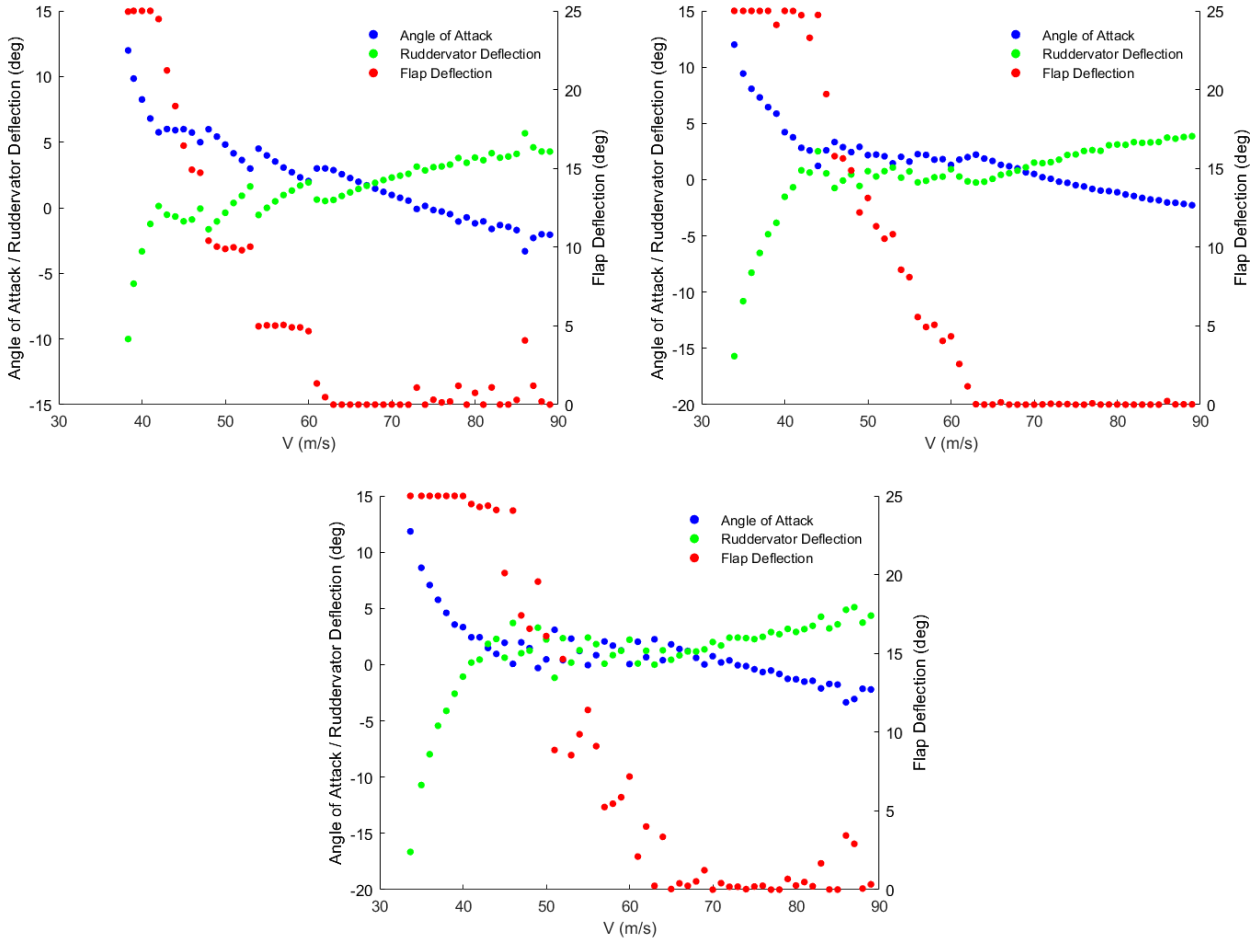


Figure 6 – Angle of attack, flap deflection, and ruddervator deflection at the lowest required aerodynamic power in trim as a function of airspeed, for OHTU (above left), ODEP (above right), and DEP+HTU (below).

and the flaps. The intention is to "absorb" the propulsive effects of DEP and HTU into high-level aerodynamic parameters, thereby encapsulating all the complexities and couplings of the original model into a simpler representation. The ruddervator deflection exhibits trends that are strongly correlated with the angle of attack, and therefore can be left out.

Figure 7 shows the trim angle of attack as a function of airspeed and flap deflection for the DEP+HTU case, along with a least-squares regression fit of the data.

The best fit is obtained by assuming that the lift coefficient is linear with angle of attack and flap deflection, with the flap effectiveness being a function of airspeed, as shown in Equation 7.

$$C_L = C_{L_0} + C_{L_\alpha}\alpha + C_{L_\alpha}\left(\tau_0 + \frac{\tau_V}{V^2}\right)\delta_\mathrm{f} \tag{7}$$

When trimmed in horizontal steady flight, lift has to be equal to the aircraft weight, and this can be used to express the trim angle of attack as a function of trim flap deflection and airspeed, as shown in Equation 8.

$$\alpha^\mathrm{tr} = \frac{\frac{2W}{C_{L_\alpha}\rho S} - \tau_V\delta_\mathrm{f}^\mathrm{tr}}{V^2} - \tau_0\delta_\mathrm{f}^\mathrm{tr} - \frac{C_{L_0}}{C_{L_\alpha}} = \frac{K_\alpha + K_V\delta_\mathrm{f}^\mathrm{tr}}{V^2} + K_\delta\delta_\mathrm{f}^\mathrm{tr} + K_0 \tag{8}$$

The $K_\circ$ coefficients can then be determined from the fit parameters, and their values can be related to the aerodynamic characteristics of the simplified model. They are reported in Table 8, together with the ones of the untrimmed clean wing for different combinations of airspeed and DEP throttle settings, from which several observations can be drawn.

Firstly, the power-off clean wing yields $\tau_V = 0$, confirming that, in the absence of propulsion, flap effectiveness is independent of airspeed, as expected from purely geometric aerodynamics. Secondly, for

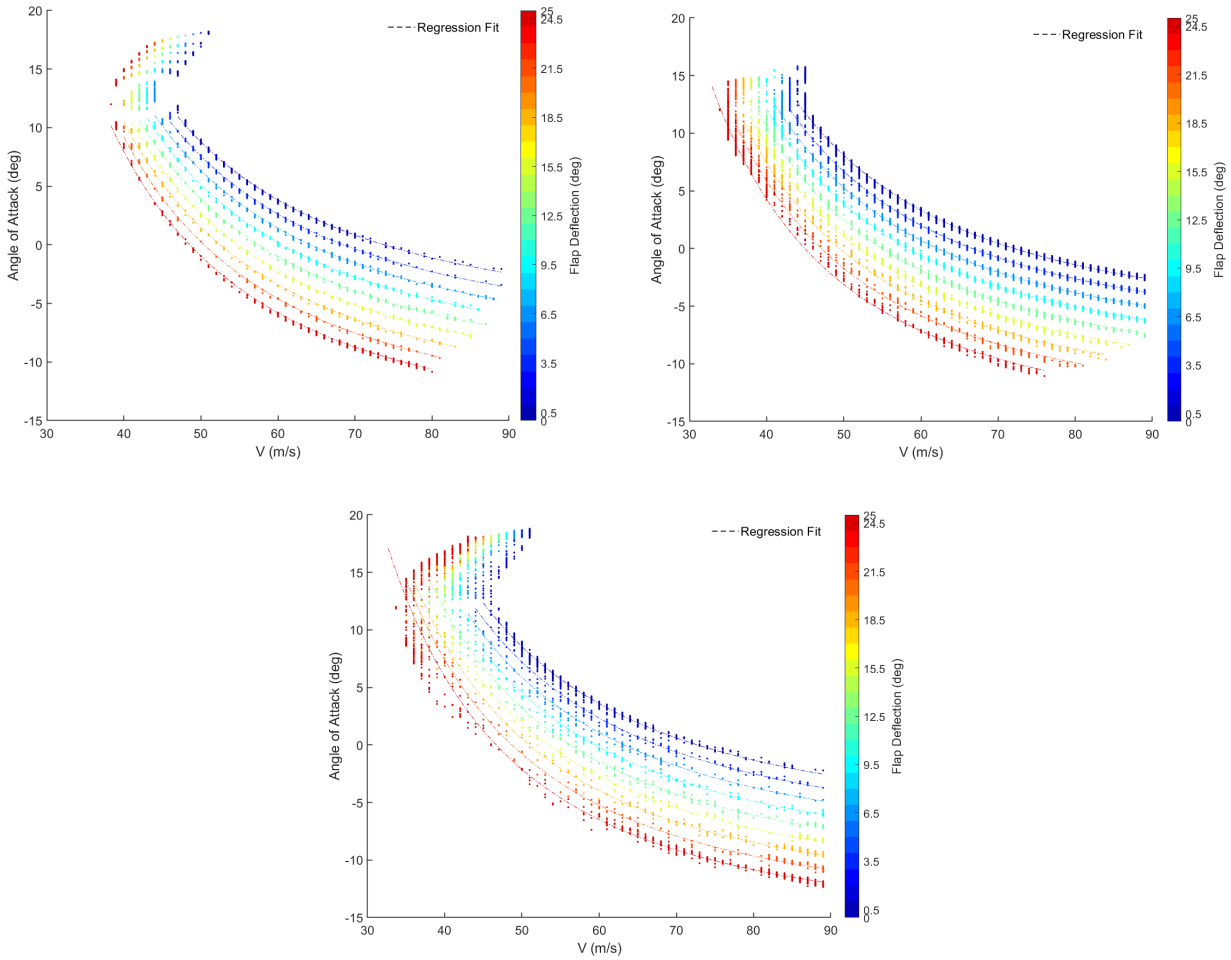


Figure 7 – Trim angle of attack as a function of airspeed and flap deflection with least-squares regression fits, for OHTU (above left), ODEP (above right), and DEP+HTU (below).

power-on cases, both C_{L_0} and C_{L_α} are higher at low speed due to the slipstream velocity ratio being significantly higher in that regime. Such airspeed dependence is not captured by the model used for the trimmed powertrains, which represents effective mean values across the entire flight envelope. Lastly, when the DEP is fully active ($\delta_{T_i} = 1$), a non-zero $\tau_V = 95.9\,\mathrm{m^2/s^2}$ indicates that the propeller slipstream introduces an airspeed-dependent component to the flap lift contribution. This value is, however, substantially lower than those fitted from the trimmed aircraft data. This could indicate that flap deployment has a considerably greater impact on the lift coefficient in trimmed flight than on the isolated clean wing, owing to its coupling with throttle scheduling, tail deflections, and the varying operating conditions across the trim envelope.

Within Figure 7, it is especially interesting to focus on the values of α^{tr} that are closest to $0\,\mathrm{deg}$ at each airspeed. In straight and level flight, such condition also means zero pitch angle and therefore a horizontal attitude of the fuselage. Figure 8 shows such values as a function of airspeed, for the three powertrains (on the left), together with the corresponding airframe lift coefficients (on the right). The latter are also shown with a piecewise linear fit based on Equation 9, whose coefficients are reported in Table 9.

$$C_L = C_{L_0} + C_{L_\alpha}\alpha \tag{9}$$

Three regions are clearly identifiable: a low airspeed region where the flap deflection is maximum and the angle of attack is positive; a moderate airspeed region where the angle of attack is close to 0 deg and the flap deflection decreases as airspeed increases; and a high airspeed region where the angle of attack is negative and the flap is completely retracted. In summary, the aircraft is able to trim at $\alpha \approx 0\,\mathrm{deg}$ in the range of $V \approx 46$–$74\ \mathrm{m/s}$ for all powertrain configurations. Outside this range, α varies linearly with airspeed due to flaps reaching saturation limits.

Table 8 – Lift-slope coefficients fit on the non-linear aircraft trim results, by powertrain configuration, with comparison to values extracted from the untrimmed clean wing.

Powertrain	Flight condition	Trimmed	C_{L_0}	C_{L_α} $(1/\mathrm{deg})$	τ_0	τ_V $(\mathrm{m}^2/\mathrm{s}^2)$
OHTU	Whole envelope	✓	0.7095	0.0976	0.3897	41.38
ODEP	Whole envelope	✓	0.7409	0.1018	0.3718	234.9
DEP+HTU	Whole envelope	✓	0.7256	0.0995	0.3679	201.7
Clean wing	$\delta_{T_i} = 0$	×	0.627	0.0817	0.483	0
Clean wing	$\delta_{T_i} = 1$, $V = 33\,\mathrm{m/s}$	×	0.999	0.0941	0.489	95.9
Clean wing	$\delta_{T_i} = 1$, $V = 80\,\mathrm{m/s}$	×	0.699	0.0839	0.489	95.9

At low airspeeds (positive α), DEP+HTU presents the highest C_{L_α}, closely followed by ODEP, which are about double the slope of the OHTU configuration (without aero-propulsive interactions). This is consistent with the strong aero-propulsive lift boost of DEP at low V, which is further amplified when HTU is active and behaving as an air break. At high airspeeds (negative α), DEP+HTU and OHTU converge to the same C_{L_α}. The DEP contribution is negligible in this regime, as the HTU provides the majority of thrust; ODEP retains a 45% higher C_{L_α} because DEP must operate at high thrust settings, sustaining stronger aero-propulsive interactions. C_{L_0} follows the same qualitative trends across powertrain configurations and speed regimes. In the moderate-speed band, the flap deflection is not saturated and is regulated together with the other trim controls to always achieve the necessary airframe lift coefficient while keeping $\alpha \approx 0\,\mathrm{deg}$.

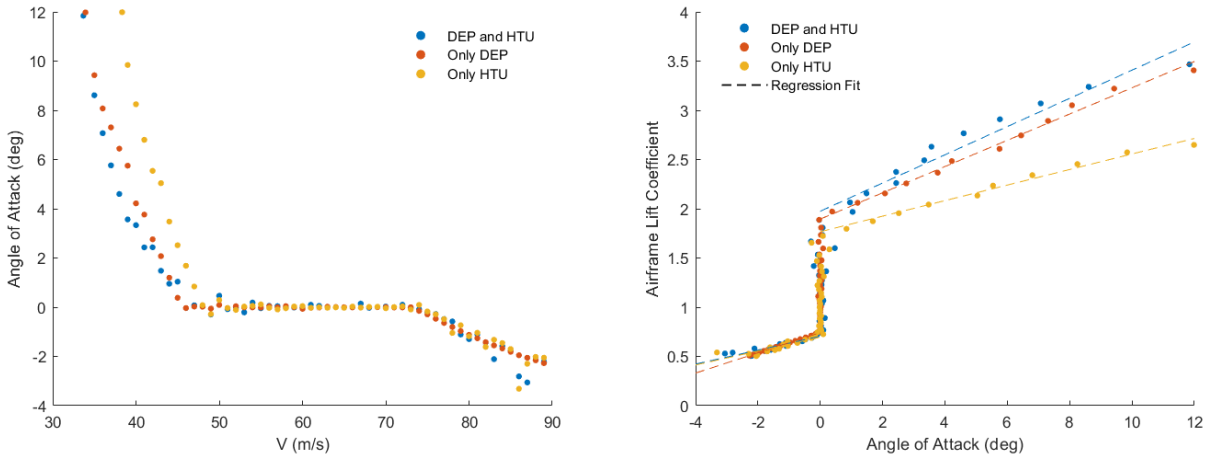


Figure 8 – Least-squares regression fit of the airframe lift coefficient as a function of the trim angle of attack, for trim solutions closest to horizontal-attitude at each airspeed.

Table 9 – Piecewise linear fit coefficients of Equation 9 for trim solutions closest to horizontal-attitude.

Powertrain	V (m/s)	C_{L_0}	$C_{L_\alpha}(1/\mathrm{deg})$
OHTU	[38, 48]	1.767	0.079
	[49, 74]	[0.77, 1.72]	—
	[75, 89]	0.696	0.071
ODEP	[34, 45]	1.895	0.133
	[46, 73]	[0.75, 1.89]	—
	[74, 89]	0.742	0.103
DEP+HTU	[34, 46]	1.975	0.143
	[47, 72]	[0.77, 1.97]	—
	[73, 89]	0.705	0.071

Similarly, the curve for minimum available power in trim, can be expressed using a reduced model

based on the parabolic drag polar assumption, as shown in Equation 10 [17].

$$P_a = \frac{1}{2}\rho V^3 S(C_{D_0} + KC_L^2) = \frac{1}{2}\rho V^3 S C_{D_0} + \frac{2KW^2}{\rho V S} = K_{D_0} V^3 + \frac{K_{D_i}}{V} \tag{10}$$

The equivalent parabolic drag-polar coefficients obtained from the least-squares fit of the trim points with minimum P_a are compared with those of the untrimmed clean airframe in Table 10. The coefficients for the clean airframe have been obtained as follows. For each propulsion system configuration and airspeed, the trimmed angle of attack corresponding to the minimum available power P_a was identified. Simulations of the clean aircraft were then performed at that angle of attack and airspeed, enabling a direct comparison of the aerodynamic coefficients between the clean and trimmed configurations at identical flight conditions. Since the trimmed angle of attack minimizing P_a at a given airspeed differs across powertrain configurations, the clean-airframe coefficient values extracted from the regression fit vary accordingly.

Relative to the clean airframe, the trimmed fit shows a slight decrease in equivalent C_{D_0}, and a marked increase in K, for all three powertrains. The reduction in C_{D_0} is counterintuitive, since trim-surface deflections usually increase drag. Although aero-propulsive interaction could reduce skin-friction drag locally, the available simulation outputs do not provide a drag breakdown; therefore, this decrease is most likely a regression artefact. The higher K indicates a very strong penalty in induced-drag for trimmed low-speed flight. As airspeed decreases, higher lift demand drives the spanwise loading farther from the elliptical optimum, increasing the rate at which induced drag grows with lift coefficient.

Table 10 – Parabolic drag polar coefficients for the clean airframe and the non-linear aircraft trimmed for minimum required aerodynamic power, by powertrain configuration.

Powertrain	Coefficient	Clean Airframe	Trimmed Aircraft	Rel. change
OHTU	C_{D_0}	5.23×10^{-2}	4.74×10^{-2}	−8.3%
	K	1.10×10^{-2}	2.32×10^{-2}	+111%
ODEP	C_{D_0}	5.40×10^{-2}	4.75×10^{-2}	−12%
	K	5.80×10^{-3}	2.09×10^{-2}	+260%
DEP+HTU	C_{D_0}	5.43×10^{-2}	4.83×10^{-2}	−11%
	K	4.30×10^{-3}	1.99×10^{-2}	+363%

5. Conclusions and Recommendations

Trim conditions in steady horizontal level flight were studied for an aircraft with a wing-mounted Distributed Electric Propulsion (DEP) and a Horizontal Tail Thrust Unit (HTU). Attention was placed on the effect of coupling both propulsion systems when trimming for different performance indicators.

Results show that using a DEP system is essential to reduce the minimum trim airspeed, while coupling DEP with the HTU has an insignificant improvement in performance regarding this parameter. Similar considerations hold for low-speed performance metrics, such as maximum endurance.

To reduce electric power consumption, trimming should be done using the HTU as the main thrust generator, when available, together with small angles of attack, flap and ruddervator deflections. These airframe trim controls remain valid for maximum range performance as well, with the powertrain architecture mainly affecting the flap deflection value required. The maximum lift-to-drag ratio significantly increases when coupling the HTU with DEP, since the HTU working in break mode allows higher DEP thrust settings and therefore higher lift generation at low airspeeds. The negative thrust generated by the HTU is not counted in the drag budget for this metric, though.

Reduced analytical models based on affine lift curve and parabolic drag polar assumptions were fitted to the trim results, showing that the trimmed aircraft has a much higher lift curve slope and a slightly higher induced-drag penalty when using DEP+HTU than the clean airframe.

Future studies should focus on exploring trim conditions for desired thrust and aerodynamic load spanwise distributions, and on studying the effect of different propulsion system sizings and placements on the trimmed performance of such category of aircraft.

6. Contact Author Email Address

mailto: C.Varriale@tudelft.nl

7. Copyright Statement

The authors confirm that they, and/or their company or organization, hold copyright on all of the original material included in this paper. The authors also confirm that they have obtained permission, from the copyright holder of any third party material included in this paper, to publish it as part of their paper. The authors confirm that they give permission, or have obtained permission from the copyright holder of this paper, for the publication and distribution of this paper as part of the ICAS proceedings or as individual off-prints from the proceedings.

References

[1] Alex M. Stoll, JoeBen Bevirt, Mark D. Moore, William J. Fredericks, and Nicholas K. Borer. “Drag Reduction Through Distributed Electric Propulsion”. In: *14th AIAA Aviation Technology, Integration, and Operations Conference* (2014).

[2] Racheal M. Erhard, Matthew A. Clarke, and Juan J. Alonso. “A Low-Cost Aero-Propulsive Analysis of Distributed Electric Propulsion Aircraft”. In: *AIAA Scitech 2021 Forum* (2021).

[3] Christopher Courtin, Ara Mahseredjian, Annick J. Dewald, Mark Drela, and John Hansman. “A Performance Comparison of eSTOL and eVTOL Aircraft”. In: *AIAA AVIATION 2021 FORUM* (2021).

[4] Justin S. Gray and Joaquim R. R. A. Martins. “Coupled aeropropulsive design optimisation of a boundary-layer ingestion propulsor”. In: *The Aeronautical Journal* 123 (2019), pp. 121–137.

[5] Karen A. Deere, Jeffrey K. Viken, Sally Viken, Melissa B. Carter, Michael Wiese, and Norma Farr. “Computational Analysis of a Wing Designed for the X-57 Distributed Electric Propulsion Aircraft”. In: *35th AIAA Applied Aerodynamics Conference* (2017).

[6] Murilo A. Gallani, Luiz Carlos S. Góes, and Luiz Augusto R. Nerosky. “Implementation of Distributed Electric Propulsion on a General Aviation Aircraft”. In: *32nd ICAS Congress* (2021).

[7] Agostino De Marco, Eugene Duke, and Jon Berndt. “A General Solution to the Aircraft Trim Problem”. In: *AIAA Modeling and Simulation Technologies Conference and Exhibit*.

[8] Carmine Varriale and Mark Voskuijl. “A trim problem formulation for maximum control authority using the Attainable Moment Set geometry”. In: *CEAS Aeronautical Journal* 13.1 (2021), pp. 251–266.

[9] Thymen Woldhuis, Salvatore Asaro, and Xuerui Wang. “Online Data-Driven Optimization of Aerodynamic Performance for an Unconventional Morphing Aircraft”. In: *AIAA SCITECH 2025 Forum* (2025).

[10] Carlo E. D. Riboldi, Stefano Cacciola, and Lorenzo Ceffa. “Studying and Optimizing the Take-Off Performance of Three-Surface Aircraft”. In: *Aerospace* 9.3 (2022).

[11] Ben Moulton, Christian Bolander, and Douglas F. Hunsaker. “Evaluation of Stability and Controllability of the Multiple Trim Solutions for a Bio-Inspired Rotating Empennage Fighter Aircraft”. In: *AIAA SCITECH 2025 Forum* (2025).

[12] UNIFIER19 Consortium. *D2.2 Final Concurrent Design Report*. Deliverable. UNIFIER19, 2021.

[13] UNIFIER19 Consortium. *D3.3.: Conceptual design report including LCA - open*. Deliverable. UNIFIER19, 2022.

[14] Lorenzo Trainelli, Carlo E.D. Riboldi, Alberto Rolando, and Francesco Salucci. “Methodologies for the initial design studies of an innovative community-friendly miniliner”. In: *IOP Conference Series: Materials Science and Engineering* 1024.1 (2021), p. 012109.

[15] Johannes S.E. Soikkeli. *Unifier C7A-HARW Flight Dynamics Simulator on Github*. 2024. URL: https://github.com/soikkelij/unifier_fds.

[16] Johannes S. Soikkeli, Drago Matko, and Thomas Koopman. “Cascaded nonlinear dynamic inversion applied to a fixed-wing distributed electric propulsion aircraft”. In: *AIAA AVIATION 2023 Forum*. eprint: https://arc.aiaa.org/doi/pdf/10.2514/6.2023-4048.

[17] Lance W. Traub. “Camber Effects on Minimum Power and Thrust Relations for Propeller Aircraft”. In: *Journal of Aircraft* 53.1 (2016), pp. 299–304.